KEK Report 97-10
UH-511-877-97
August 1997
A/H

A Generator for Study of Background due to Beam-gas Interaction at KEK B-factory

S.K. SAHU

High Energy Accelerator Research Organization

** From April 1, 1997, **High Energy Accelerator Research Organization (KEK)** was newly established. The new organization is restructured of three reseach institutes, National Laboratory for High Energy Physics (KEK), Institues of Nuclear Study (INS), Univ. of Tokyo and Meson Science Laboratory, Faculty of Science, Univ. of Tokyo.*

KEK Reports are available from:

Information Resources Division
High Energy Accelerator Research Organization (KEK)
1-1 Oho, Tsukuba-shi
Ibaraki-ken, 305
JAPAN

Phone: 0298-64-5137
Fax: 0298-64-4604
Cable: KEK OHO
E-mail: Library@kekvax.kek.jp (Internet Address)
Internet: http://www.kek.jp

A Generator for Study of Background due to Beam-gas Interaction at KEK B-factory

S. K. Sahu*

Department of Physics & Astronomy
University of Hawaii, Honolulu, HI-96822, U.S.A.
&
KEK, High Energy Accelerator Research Organization
1-1, Oho, Tsukuba, 305, Japan

Abstract

A spent-electron generator based on DECAY TURTLE has been prepared for study of beam-gas background at the KEK B-factory. Methods have been described in detail. Basic studies of background rate and its dependence on various accelerator parameters have been performed.

1 Introduction

Beam pipes in high energy storage rings do not have an ideal vacuum. As a result, the circulating particles sometimes interact with the residual gas molecules, and hence deviate from their ideal path. In an e^+e^- storage ring such particles are called spent electrons(or positrons). In this note, where we concern ourselves to the KEK B-factory, which is an asymmetric e^+e^- collider, we will refer to both spent electrons and positrons as just *spent electrons*. A considerable fraction of these spent electrons, while swimming through the beam line elements may deviate quite a lot from their original path, and finally hit the detector, thus causing a background problem.

Such backgrounds are rather severe in high luminosity machines, such as B-factories, since they cause *Radiation Damage* to detector components, increase *trigger rates*, and may even overlap on real physics events one is interested in, thereby ruining the kinematics of the genuine event. Secondary shower produced by these spent electrons make the situation only worse.

The aim of this work is to provide a spent electron generator which detector physicists at KEK B-factory can use for estimating backgrounds for different sub-detectors. This study would also give hints as to which accelerator paramaters/masks might need improvement as far as background issues are concerned. Detailed descriptions about the KEK-B accelerator and its detector BELLE may be found in [AccDR, BelleTDR].

Initial studies in BELLE in this direction have been done by [OzakiH, SahuSK]. This report is about a more comprehensive and somewhat independent study in the same direction.

The procedure is quite straight-forward. First, we simulate the beam-profile in the straight sections of the electron and positron rings of the KEK B-factory. These simulated beam particles are then swum through a *modified version* of the program DECAY TURTLE [Turtle] until a point where the particle may interact with a residual gas molecule. The interaction may be of first order (Coulomb scattering) or second order (Bremsstrahlung) in α (electromagnetic coupling constant $= e^2/4\pi = 1/137$ in natural units). The particle with altered (four)momentum then continues its journey through the beam line with the help of DECAY TURTLE until it reaches the BELLE detector.

At this point the position and 4-vector information may be introduced to the BELLE Geant simulation for a complete evaluation of the effects of the background.

In the next section, we discuss the issue of residual gas in an accelerator beam-pipe. In the third section we give a description of beam parameters of the KEK B-factory relevant to this generator. In the fourth section we discuss the physics of beam-gas scattering and sampling methods. In the fifth section, we describe the beam-propagation by the program, and in the final section we show some results.

*E-mail:sahu@uhheph.phys.hawaii.edu

2 Residual Gas in the Beam-pipe

Technically, it has never been possible to achieve perfect vacuum in the beam pipes of high energy storage rings. When one tries to create an excellent vacuum inside the beam pipe by pumping out all the gas molecules he can, and contends at the vacuum monitor reading, a great many of them remain adsorbed on the wall. Once the beam is turned on, they start getting kicked off the wall (*i.e., desorbed*) by the synchrotron radiation from the beam, thus deteriorating the vacuum. Certain remnant oxide layers inside the beam-pipe have some carbon compounds, and are capable of forming and accomodating CO molecules. When illuminated with synchrotron photons, they release, or *desorb* them. It is known that most of the residual gas is CO. The *desorption* gradually decreases with increasing synchrotron irradiation, and finally attains a stable value, after a reasonable time of machine operation.

In a practical machine, therefore, one tries to achieve good vacuum by (1) reducing the synchrotron radiation by using bending magnets of large radius of curvature; (2) increasing the pumping speed; and (3) fine polishing the inner wall of the beam pipe, so that surface area available for adsorption is minimal. The first point is often not negotiable because of higher priorities imposed by other practical aspects of accelerator, such as available circumference and cost. Number of available vacuum ducts limit the pumping speed. Surface polish, although can be excellent, still has a limit. Therefore, for a storage ring, the best achievable vacuum is a limited and calculable quantity.

Average pressure in the ring is easily calculated to be[†]

$$P = \frac{\eta_D n_\gamma}{KS}, \tag{1}$$

where P is the pressure in Torr[‡], η_D is the *desorption coefficient* in molecules per photon, meaning how many gas molecules are desorbed per synchrotron photon, n_γ is the linear synchrotron photon density existing in the pipe in photons/sec/m, S is the distributed pumping speed in lit/sec/m, and K is the conversion factor 3.24×10^{19} molecules/Torr/lit.

In KEK B-factory, for the positron ring for example, $n_\gamma = 3.3 \times 10^{18}$ photons/sec/m, $\eta_D = 10^{-6}$ molecules/photon, and a reasonably achievable pump speed is of the order of 100 lit/sec/m [AccDR]. Putting these numbers in Equation 1, one gets a pressure of the order of 10^{-9} Torr during the normal machine operation. This kind of pressure corresponds to about 30 molecules in a 100 μm cube. These numbers are similar for the electron ring as well.

3 Beam parameters at KEK B-factory

KEK B-factory is an asymmetric e^+e^- collider parameters of which are given in Table 1. The straight sections of the positron ring (henceforth called Low Energy Ring, or LER) and the electron ring (henceforth called High Energy Ring, or HER) are 20 meters and 50 meters, respectively.

Beam particles are swum through the beam line, parameters of which are given in Tables 2 and 3, for LER and HER, respectively.

Meaning of the parameters are as follows :

Name is the mnemonic of the element of the beam line. **IP** stands for the interaction point. **DRIFT** indicates a drift space without any electromagnetic field. Mnemonics starting with **B** indicate a bending magnet, and those starting with **Q** indicate a quadrupole focussing or defocussing magnet.

Length stands for the length of that element along the beam axis in meters.

Z_{length} stands for the distance of the edge of that certain element from the interaction point.

[†]**Residual Gas Pressure :** Consider a section of beam pipe of length l and arbitrary cross-section. Then number of molecules escaping from the wall per second = $n_\gamma \eta_D l$ molecules/sec = $\frac{n_\gamma \eta_D l}{N_A}$ moles/sec where N_A is Avogadro's number. The volume that these many molecules aquire under pressure $P = \frac{RT}{P} \cdot \frac{n_\gamma \eta_D l}{N_A}$ m^3, where R is the universal gas constant (= 8.31 Joule/mole/°K), and T is the temperature in $°K$, according to the ideal gas law $PV = nRT$. In equilibrium, in each second this volume would be swept away by the pump. In terms of pump speed, this volume becomes $Sl \times 10^{-3}$ m^3. Equating the above two volumes, one gets, for pressure P in Torr, $P = \frac{n_\gamma \eta_D}{S} \cdot \frac{RT}{N_A \cdot 10^{-3} \cdot 133.32}$ The factor K is then 3.24×10^{19} molecules/Torr/lit.

[‡]1 Torr = 1 mm of Hg = 1/760 atmosphere = 133.32 N/m^2

Value gives the value of that certain element – for drift space it is just the length in meters; For bending magnet it is equal to $B \times L/(3.3356 * E_{beam})$; and for quadrupoles it is equal to $\partial B/\partial r \times L/(3.3356 * E_{beam})$, where L is the length of the element in meter, E_{beam} is the design energy of the beam particle in GeV, B is the magnetic field in Tesla, and $\partial B/\partial r$ is the radial variation of magnetic field in Tesla/m.

β_x is the horizontal β-function of the beam, which (sort of) gives the extent of focus at that certain point on the beam line.

α_x is the derivative of β_x along the beam direction. If we know $\beta_x(0)$ and $\alpha_x(0)$ at $z = z_0$, then we can calculate β_x at z by :

$$\beta_x = \beta_x(0) + 2 * \alpha_x(0) * (z - z_0) + ...$$

It is important to know that in case of KEK B-factory, the horizontal and vertical *Emittances*[§] are measured in meters. The horizontal and vertical beam spreads are given by $\sigma_x = \sqrt{\beta_x * \epsilon_x}$ and $\sigma_y = \sqrt{\beta_y * \epsilon_y}$, respectively.

In order to reduce the backgrounds, some masks(slits) have been designed be placed in the beam line. Their positions and apertures are given in

Table 4. They are retractable, and therefore may have different apertures during run-time and fill-time.

We wanted, first of all to ascertain that given the initial beam profile, the TURTLE optics reproduces the beam shapes and betatron amplitudes as prescribed in the accelerator design. We checked the betatron oscillations x' and y' as well as beam profiles σ_x and σ_y, and all of those are in close agreement with the numbers independently calculated by the KEK-B accelerator designers. For the sake of comparison, in Tables 5 and 6, we show the beam profiles as prescribed with the numbers from our TURTLE simulation at every optical element. The disagreement of the profiles at the interaction point is attributed to the fact that the final focussing quadrupoles are not optimized yet, and a small change in the field would affect the final focus at IP a lot. In any case, it does not pose any serious problem to our calculation.

4 Beam-gas Scattering Mechanisms

Electromagnetic interaction[¶] of the beam particle with the residual gas molecule can be of the first order (Coulomb scattering) or second order (Bremsstrahlung). Feynman diagrams for these processes are given in Fig.1. Interaction of the beam particle with the valence electron cloud of the residual molecule is negligible compared to that with the nucleus. We will therefore consider interactions with the residual gas nuclei only.

4.1 Coulomb Scattering

Classical Coulomb scattering cross-section for an electron of velocity β and momentum $|\vec{p}|$ hitting a nucleus of charge Z is given by[‖]

$$\frac{\mathrm{d}\sigma}{\mathrm{d}\Omega} = \frac{Z^2\alpha^2}{4\beta^2 |\vec{p}|^2 \sin^4 \frac{\theta}{2}}. \tag{2}$$

The singularity in the scattering angle θ demands that we impose a minimum angle cut θ_c while making total cross-section calculations. With high energy approximations $\beta \approx 1$, $|\vec{p}| \approx E$ and small angle approximation (θ_c would be of the order of 1 mRad, for example, as will be discussed later) $\sin\theta \approx \theta$, we deduce

$$\sigma_{\theta_c \to \theta_2} = \frac{4\pi Z^2\alpha^2}{E^2} \left[\frac{1}{\theta_c^2} - \frac{1}{\theta_2^2}\right], \tag{3}$$

[§]The unit of emittance is conventionally meter·radian, since it is defined as the area of the phase space in $x - x'$ or $y - y'$ containing 90% of the beam bunch. This convention is set by proton rings and linear accelerators where the beam profile is elliptical. The emittance in their case is, of course, in meter·radian with a factor of π explicitly written out. In case of electron synchrotrons, however, the beam profile becomes Gaussian because of continuous synchrotron loss. In that case, one defines the emittance as the area in $x - x'$ or $y - y'$ phase space containing all particles in a bunch within 2σ deviation ***divided by*** π ***radian***. That's why the unit of emittance here is ***meter***.

[¶]Deep Inelastic Scattering(DIS), where the beam electron sees the internal structure of the gas nucleus and breaks it apart, is not considered here, since that cross-section is much smaller than the ones considered in this section at these energies.

[‖]see for example, QED by W. Greiner, Springer-Verlag.

where θ_2 is a larger angle cut. Since $\theta_c^2 \ll \theta_2^2$, we get the Coulomb scattering (approximate) cross-section :

$$\sigma_{\theta_c} = \frac{4\pi Z^2\alpha^2}{E^2} \cdot \frac{1}{\theta_c^2} \tag{4}$$

We would like to take a moment to note that the quantum mechanical counterpart of Coulomb scattering is called *Mott* scattering, which bears the cross-section** :

$$\frac{\mathrm{d}\sigma}{\mathrm{d}\Omega} = \frac{Z^2\alpha^2(1-\beta^2\sin^2\frac{\theta}{2})}{4\beta^2\left|\vec{p}\right|^2\sin^4\frac{\theta}{2}}. \tag{5}$$

Using the same approximations as above, we get the integrated cross-section :

$$\sigma_{\theta_c\to\theta_2} = \frac{2\pi Z^2\alpha^2}{E^2}\left[\ln\theta_c + \frac{2}{\theta_c^2} - \ln\theta_2 - \frac{2}{\theta_2^2}\right]. \tag{6}$$

First, 3rd and 4th terms in the square bracket contribute less than 0.01% for small θ_c ($\sim$ 1 mRad). This formula then reduces to the simple non-relativistic Coulomb scattering formula.

We therefore stick to the non-relativistic formula, and use its exact form during the Monte Carlo generation of the scattering :

$$\frac{\mathrm{d}\sigma}{\mathrm{d}\Omega} = \frac{Z^2\alpha^2}{4E^2\sin^4\frac{\theta}{2}}, \tag{7}$$

which is synonymous with Eqn. 2 at the high energy we are dealing with.

Total cross-section is obtained with the formula above with

$$\int_{\theta=\theta_c}^{\pi}\int_{\phi=0}^{2\pi}\frac{\mathrm{d}\sigma}{\mathrm{d}\phi\sin\theta\mathrm{d}\theta}. \tag{8}$$

Polar angle is sampled with the relation :

$$\frac{\mathrm{d}\sigma}{\mathrm{d}\theta} \propto \frac{\sin\theta}{\sin^4\frac{\theta}{2}}, \tag{9}$$

and ϕ is sampled uniformly over the range $[0, 2\pi]$.

4.2 Bremsstrahlung

Unlike Coulomb scattering, Bremsstrahlung is a second order process and the cross-sections are sensitive to atomic form factors. In such a rarefied medium one talks of *discrete* bremsstrahlung, the Coulomb-corrected cross-section of which is given by the famous Bethe-Heitler formula[BetheH, HeitlerW, SegreE], and rearranged in[KochMotz] and by Patrick and Urban in [GeantM] :

$$\begin{aligned}\frac{d\sigma(Z,E,\epsilon)}{d\epsilon} &= \frac{r_0^2\alpha Z[Z+\xi(Z)]}{\epsilon}\Big\{\left[1+(1-\epsilon)^2\right]\left[\Phi_1(\delta)-F(Z)\right] \\ &\quad -\frac{2}{3}(1-\epsilon)\left[\Phi_2(\delta)-F(Z)\right]\Big\}\end{aligned} \tag{10}$$

where, E is the incident electron energy, Z is the atomic number of the target, ϵ is the fraction of E carried away by the photon, r_0 is the classical electron radius ($=e^2/m_ec^2 = 2.82\times10^{-13}$ cm). Φ and f_C are the screening and Coulomb correction functions, respectively, as defined below :

$$\delta = \frac{136m_e}{Z^{1/3}E}\cdot\frac{\epsilon}{1-\epsilon}$$

$$\left.\begin{aligned}\Phi_1(\delta) &= 20.867 - 3.242\delta + 0.625\delta^2 \\ \Phi_2(\delta) &= 20.209 - 1.930\delta - 0.086\delta^2\end{aligned}\right\} \quad \delta \le 1$$

**see for example, QED by W. Greiner, Springer-Verlag.

$$\Phi_1(\delta) = \Phi_2(\delta) = 21.12 - 4.184\ln(\delta + 0.952) \quad \text{for} \delta > 1$$

$$F(Z) = \begin{cases} 4/3\ \ln Z & E < 0.05\ \text{GeV} \\ 4/3\ \ln Z + 4f_c(Z) & E \geq 0.05\text{GeV} \end{cases}$$

$$\xi(Z) = \frac{\ln(1440/Z^{2/3})}{\ln(183/Z^{1/3}) - f_c(Z)}$$

$$f_c(Z) = Z\alpha\left\{\frac{1}{1+Z\alpha} + 0.20206 - 0.0369Z\alpha + 0.0083(Z\alpha)^2 - 0.002(Z\alpha)^3\right\}$$

ϵ is bounded by

$$\epsilon_c \equiv \frac{k_c}{E} \leq \epsilon \leq 1 - \frac{m_e}{E} \sim 1, \tag{11}$$

where k_c is the photon cut-off energy and ϵ_c is the scaled photon cut-off energy. In our simulations, it is typically $0.001 \sim 0.05$ (this issue will be discussed later).

This formula has been numerically integrated, and a parametric form has been available as the routine GBRSGE, coded in [GeantM]. We use a modified version of that routine to calculate the total cross-section.

Sampling of the photon energy is a bit difficult because of the lengthy form of the cross-sectional formula. So we simplified Eqn. 10 a little as follows :

Assuming $Z = 7$[††], we get :

$$\begin{aligned} f_c(Z) &= 1.01 \\ \xi(z) &= 1.86 \\ F(Z) &= 6.6 \end{aligned}$$

The classical electron radius $r_0 = 2.8$ fm $= 14.3/\text{GeV}$.

Putting all these vales in Eqn. 10, we get

$$\frac{d\sigma}{d\epsilon} = \frac{92.6}{\epsilon}\left\{\left[1 + (1-\epsilon)^2\right]\left[\Phi_1(\delta) - 6.6\right] - \frac{2}{3}(1-\epsilon)\left[\Phi_2(\delta) - 6.6\right]\right\} \tag{12}$$

We sample the photon energy with this formula.

Incorporation of the polar angle of the photon in sampling is difficult, again because of the complexity of the formula. The differential cross-section is given by [Tsai] :

$$\begin{aligned} \frac{d\sigma}{dkd\Omega} = \frac{2\alpha^2 e^2}{\pi k m_e^4}\Bigg\{&\left[\frac{2\epsilon - 2}{(1+u^2)^2} + \frac{12u^2(1-\epsilon)}{(1+u^2)^4}\right] Z(Z+1) \\ &+ \left[\frac{2 - 2\epsilon - \epsilon^2}{(1+u^2)^2} - \frac{4u^2(1-\epsilon)}{(1+u^2)^4}\right]\left[X - 2Z^2 f_c((\alpha Z)^2)\right]\Bigg\} \end{aligned} \tag{13}$$

where

$$\begin{aligned} u &= \frac{E\theta}{m_e} \\ X &= \int_{t_{min}}^{m_e^2(1+u^2)^2} [G_Z^{el}(t) + G_Z^{in}(t)]\frac{t - t_{min}}{t^2}dt \\ t_{min} &= \left[\frac{k m_e^2(1+u^2)}{2E(E-k)}\right]^2 = \left[\frac{\epsilon m_e^2(1+u^2)}{2E(1-\epsilon)}\right]^2 \end{aligned} \tag{14}$$

G_Z^{el} and G_Z^{in} are the elastic and inelastic form factors respectively.

[††]In TRISTAN experiment at KEK, we observed that the residual gas consisted mostly of carbon monoxide, CO. Average atomic number then becomes 7.

This formula is too tedius to handle, and it is unnecessary to do so. A crude simplification of this formula immediately shows that

$$\frac{\mathrm{d}\sigma}{\mathrm{d}\omega} \propto \frac{1}{\theta^6}. \tag{15}$$

This is two degrees down compared to the case of Coulomb scattering, and the proportionality factor is much smaller, being scaled by $(\frac{m}{E})^6$. Therefore we make the assumption that the photon is emitted collinear to the initial electron(positron) beam.

4.3 Sampling

4.3.1 Coulomb Scattering

Let's consider the Coulomb scattering first. Only θ and ϕ need to be sampled in this case. Energy of the electron does not change. ϕ is sampled uniformly as described before. But θ has a singularity (Eqn. 2), and therefore *acceptance-rejection* method becomes inefficient for very low θ_c. Luckily, the formula is simple enough to be integrated and taken an inverse of. So we make use of the *distribution inverse* method for sampling θ. The method is described below :

Let the differential cross-section be respresented by the *density function* $f(x)$, normalizable with the relation

$$\int_{-\infty}^{\infty} f(x)\mathrm{d}x = 1. \tag{16}$$

The cumulative probability or the *distribution function* $F(x)$ is then given by

$$P = F(x) = \int_{-\infty}^{x} f(x)\mathrm{d}x. \tag{17}$$

For random sampling, $P = F(x)$ varies uniformly between 0 and 1. Therefore the algorithm becomes :

1. Sample a uniform random number R ($= F(x)$).
2. $x = F^{-1}(R)$ is the desired sample.

In other words, x's chosen in this way will be distributed like $f(x)$, which is what we want.

For Coulomb scattering (Eqn. 2),

$$f(\theta) = \frac{\mathrm{d}\sigma}{\mathrm{d}\theta} = A \cdot \frac{\sin\theta}{\sin^4\frac{\theta}{2}}. \tag{18}$$

Therefore

$$\begin{aligned} F(\theta) &= A \cdot \int_{\theta_c}^{\theta} f(\theta)\mathrm{d}(\theta) \\ &= 2A \cdot \left\{ \frac{1}{\sin^2\frac{\theta_c}{2}} - \frac{1}{\sin^2\frac{\theta}{2}} \right\} \end{aligned} \tag{19}$$

$$\tag{20}$$

Then θ can be obtained by inverting the above equation, namely :

$$\theta = 2 \cdot \sin^{-1}\left\{ \left[-\frac{F(\theta)}{2A} + \frac{1}{\sin^2\frac{\theta_c}{2}} \right]^{-\frac{1}{2}} \right\}. \tag{21}$$

The normalization constant A is determined by

$$F(\pi) = 1 \Longrightarrow 2A \cdot \left\{ \frac{1}{\sin^2\frac{\theta_c}{2}} - \frac{1}{\sin^2\frac{\pi}{2}} \right\} = 1. \tag{22}$$

The θ distribution obtained for positrons in this process is plotted(histogram) in Fig.2(a). The dotted line that closely follows the distribution is the $1/x^3$ curve, which should be good for small angles, for the sake of comparison. It is plotted only for the sake of comparison.

4.3.2 Bremsstrahlung

As discussed before, we do not sample θ, and assume the final electrons' direction is the same as the initial one. Hence there is no need to sample ϕ, either. We just have to sample the photon energy according to Eqn. 12. This formula, although can be integrated easily, cannot be conveniently inverted after integration, as can be readily seen from its functional form. We therefore do not use the distribution inverse method simlilar to Coulomb scattering case, rather use the *acceptance-rejection* method, which has worse efficiency, but seems to be our only easy way out. We will describe the *acceptance-rejection* method here :

1. Let the differential cross-section be represented by the *density function* $f(x)$ where $x \in [0,1]$, and $f(x)$ is less than a constant f_0 throughout the range.
2. Sample two uniform random numbers R and x in the range $[0,1]$.
3. If $R \cdot f_0 \leq f(x)$ then accept x. Else goto step 2.

This method has been utilized to sample the photon energy using Eqn. 12. Plotted in Fig.2(b) (histogram)is the positron energy spectrum in GeV ($E_{beam} \cdot (1-\epsilon)$), with $\epsilon_c = 0.05$. The dotted line is the $1/\epsilon$ function that is popularly used for Bremsstrahlung spectrum. A small discrepancy is seen because of all the corrections in Eqn. 12.

5 Beam Propagation

The beam profile is sampled at the beginning of the straight sections with the information given in Table 1. The sampling is done in both emittance planes, *i.e.*, $x - x'$ and $y - y'$ planes simultaneously. Positions and four-vectors are then used as inputs to Decay Turtle.

Decay TURTLE(**T**race **U**nlimited **R**ays **T**hrough **L**umped **E**lements) is a charged particle transport program created by Brown and Iselin [Turtle]. It takes a charged particle and propagates it through a predefined lattice of magnetic elements, such as dipole, quadrupole, sextupole and field-less drift spaces. It can also handle horizontal, vertical and elliptical masks(slits) which can be used to chop off a certain part of the tail of the beam, if desired.

A feature of Decay TURTLE allows decay of charged particles during propagation. This feature was intended to be used for $\pi^{\pm}$ beam lines where the $\pi^{\pm}$ may decay into $\mu^{\pm}$ and neutrinos. We use this feature to incorporate our scattering mechanisms. We make the "decay"(interaction) probability uniform along the beam-line, assuming *uniform* gas pressure in the beam pipe. When the scattering switch is on, each generated particle must undergo a scattering before it reaches the BELLE detector.

Graphic representaions of tracks of (spent) electrons and positrons are given in Figs. [3 – 5]. In all these pictures, horizontal axis gives the position in z(beam direction) and the vertical axis gives the $x-$position of the beam(profile parallel to ground). The unscattered propagation of e^+ and e^- beams, *i.e.* when neither Bremsstrahlung not Coulomb scattering is present, is shown in Fig. 3. In Fig. 4 we show the propagation of the two beams with only Bremsstrahlung scattering taking place somewhere along the beam-pipe. Run-time parameters are used. Effect of the slits in stopping some of the off-momentum particles is also seen. In Fig. 5 we show the propagation of the two beams with only Coulomb scattering taking place somewhere along the beam-line. Again, run-time parameters are used.

In Figs. [6 – 8] we show the same propagation profiles as for the cases in Figs. [3 – 5], except that injection-time parameters are used. The beam is therefore broad, and masks drawn out.

6 Spent Electron Profiles at BELLE and Results

A proper estimation of the background seen by the BELLE detector is possible only when a full Geant simulation of the spent particles is done. While such a study is being pursued by several groups at the moment, (calculations of background at the BELLE Time of Flight TOF system will be presented later in this section as an example) we decided to make a generator level estimation of spent electron background by looking at profiles of spent particles in or near the detector.

6.1 x–y Profile

Spent particle profile for e^+ Bremsstrahlung at the IP of BELLE are shown in Fig. 9(a). It may be seen that the profile is flatter in the horizontal plane(x–plane), which is not unusual, since these particles are expected to more or less follow the beam-profile(and the same optics, of course !). This conjecture is tested by making the beam flat in the y–plane at the beginning - and the profile is seems to follow it as is observed in Fig. 9(b).

In order to have a qualitative estimation of the background and study the effect of beam optics, we decided to quantify the beam profile at the interaction point as a measure of the background. If the spent particle is more that 2 cm away from the IP at the vertical plane containing the IP ($r > 2$ cm), then we call it a "Hit" in the detector. Background rates are then calculated in Hz for different scattering mechanisms (and added together) and for different beam optical configurations.

6.2 Determination of Physical Cut Values

Using this criterion we first studied the effect of physical cuts : ϵ_c (scaled photon energy cut) for Bremsstrahlung process, as discussed in 4.2 and θ_c (minimum scattering angle cut) for Coulomb scattering process, as discussed in 4.1 . Events were generated using different cut values, and using the criterion above, number of hits were calculated. The results are plotted in Fig. 10. It is clearly seen that below a certain value of cut for every process, the hit rate saturates. Hence a safe cut value may be chosen by looking at these plots. The cut values that we generically use for all our background study are given in Table 7.

6.3 z–origin of Spent Particles

It is sometimes important to know where the majority of spent particles that hit the detector originate in the length of the beam pipe. With the criterion for a "hit" as described above, we plot in Fig. 11 the z-position of scattering of these particles off the beam-gas. Fig. 11(a),(b),(c) and (d) give z-position distribution of the origin of hitting particles for e^+ Bremsstrahlung, e^+ Coulomb, e^- Bremsstrahlung and e^- Coulomb scattering processes, respectively. BELLE detector is situated at the right-most end of each of these plots. For comparing the position with corresponding beam-elements, beam-line plots similar to Figs. [3 – 8] are given at the bottom of these histograms in the same figure. It is observed that while Coulomb scattered e^+/e^- come from nearby regions of BELLE, Bremsstrahlungs come from all over the straight section. In general, improving vacuum near the detector as much as possible would help reduce the background.

6.4 Effect of Mis-aligned Optics

It is not to be expected that all the beam elements will be aligned properly at the beginning of the experiment. Therefore we have estimated the effect of small mis-alignments of optical elements on beam backgrounds. Typically, as long as the beam elements are not off by more than 2 mm from the designed beam-line, the backgrounds from different sources do not exceed by more than 50% from their normal values. As an example. we show the effects of shifts $(\Delta x, \Delta y)$ of closest and farthest quadrupoles to BELLE in the LER on background rates. Factor by which the background increases is plotted as a function of Δx and Δy in Fig. 12. Shifting of closest quad to BELLE yields Fig. 12(a), and (b) represents shifting of the farthest quad from BELLE in the straight section, both in LER.

6.5 Background Profile at BELLE-TOF

As an illustration of the utility of this generator to the calculation of background in BELLE detector, we present some results pertaining to the BELLE-Time of Flight (TOF) detector. The TOF surrounds the beam-pipe, silicon vertex detector, central drift chamber and the aerogel Čerenkov counter. We plot in Fig. 14 the distributions of photon and charged particle flux entering the TOF due to all background processes in a period of 10 milli-sec. The azimuthal distribution (14a) clearly follows the beam shape. Energy distribution (14c) warns us that a non-negligible flux of high-energy gammas enter the BELLE detector due to secondary showers from the spent particles. Energy-weighted distribution of z-origin of photons (14d) has several peaks, which exactly correspond to the positions of heavy materials like flanges, masks and tapers along

the beam-pipe in the interaction region. Such materials behave as "photon amplifiers (!)" to backgrounds. Hence one must try to reduce the amount of heavy materials around the beam-pipe as much as possible. Charged particle distributions are shown in Figs. 14(e & f) for the sake of comparison and establish the fact that charged particle flux is quite small, and is not likely to cause any serious concern to trigger efficiency.

Acknowledgement

The author is grateful to Andrzej Bozek, Hitoshi Ozaki and Shoji Uno of KEK for providing many suggestions and corrections to this work. Nobu Toge has helped by providing the author with many useful informations on accelerator parameters. Extensive use of CERN Program Library and KEK computing facility has been made. The work has been supported by the U.S. Department of Energy grant DE-FG03-94ER40833.

References

[AccDR] KEK B-Factory Design Report, June 1995.

[BelleLOI] Letter of Intent, BELLE Collaboration, 1993

[BelleTDR] Technical Design Report, BELLE Collaboration, 1995.

[BetheH] H. Bethe and W. Heitler, Proc. Roy. Soc. A146(1934)83.

[GeantM] *GEANT* CERN Library Long Writeup W5013, June 1993.

[HeitlerW] *Quantum Theory of Radiation* (Oxford, 1954), 3rd Ed., p. 244.

[KochMotz] H. W. Koch and J. W. Motz, Rev. Mod. Phys 31(1959)920.

[OzakiH] H. Ozaki, BELLE Note 57 (March 1995).

[SahuSK] S.K. Sahu, BELLE Note 90 (October 1995).

[SegreE] E. Segre, *Experimental Nuclear Physics* (John Wiley, 1953), p. 260.

[Tsai] Y. S. Tsai, Rev. Mod. Phys.,46(1974)815; *ibid*, 49(1977)421.

[Turtle] K.L. Brown and Ch. Iselin, *DECAY TURTLE*; CERN Library Long Writeup, CERN 74-2.

e^+ energy	3.5 GeV
e^- energy	8.0 GeV
e^+ current	1.1 Amp
e^- current	2.6 Amp
Targeted vacuum	1 nanotorr
β_x at IP	0.33 meter
β_y at IP	0.01 meter
ϵ_x	1.8×10^{-8}
ϵ_y	3.6×10^{-10}
ϵ_x at injection	1.3×10^{-5}
ϵ_y at injection	1.3×10^{-6}

Table 1: Relevant parameters of KEK B-factory

Name	Z_{length}	Length	Value	α_x	β_x	α_y	β_y
IP	0.0000	1.68500	1.72780	0.0000	0.3300	0.0000	0.0080
QCSR	1.6850	0.50000	-0.73658	-5.1160	9.2721	211.2400	369.1400
DRIFT	2.1850	3.31500	3.35740	-18.3750	18.0650	-83.2550	428.8300
QC2I	5.5000	0.50000	0.14802	-81.1800	352.2900	-28.8890	51.2830
QC2I2	6.0000	0.50000	0.14802	-28.7480	408.6600	-16.7460	29.0130
DRIFT	6.5000	5.77000	5.77000	31.9900	407.0000	-9.6839	16.1150
QC3I	12.2700	0.46200	-0.17157	17.4690	121.6500	24.2480	100.1400
DRIFT	12.7310	2.25500	2.25500	-2.8461	114.9000	6.8614	114.7500
QC4I	14.9860	0.46200	0.16599	-3.0246	128.1300	7.8059	147.8100
DRIFT	15.4480	2.05600	2.05600	17.4800	121.4700	34.7290	167.1900
QC5I	17.5040	0.46200	-0.18805	12.2890	60.2410	49.5790	340.5900
DRIFT	17.9660	0.40000	0.40000	1.2659	54.1580	-15.8850	356.6400
BX5I	18.3660	0.30000	-0.00300	1.2467	53.1520	-15.6010	344.0400
DRIFT	18.6660	0.40000	0.40000	1.2323	52.4090	-15.3960	334.7400
BX4I	19.0660	2.50000	-0.05208	1.2131	51.4310	-15.1110	322.5400
DRIFT	21.5660	0.40000	0.40000	1.0930	45.6680	-13.5940	250.6800

Table 2: Parameters of the LER Version 230 95/06/28

Name	Z_{length}	Length	Value	α_x	β_x	α_y	β_y
IP	0.0000	1.35000	1.35860	-1.0E-12	0.3300	0.0000	0.0080
QCSLA	1.3500	0.50000	-0.42218	-4.11100	5.9221	-169.6000	230.5900
QCSLB	1.3500	0.50000	-0.42218	-6.74380	8.8336	-136.5000	314.7900
DRIFT	1.8500	1.15040	1.15830	-19.09300	45.7850	-113.8200	598.7400
QC1EL	3.0004	0.30000	-0.15428	-30.46200	60.4790	-20.1900	639.5800
QC1EL2	3.3004	0.30000	-0.15428	-47.95100	83.7000	77.1250	622.2300
DRIFT	3.6004	2.60000	2.60000	-119.41000	518.8300	52.2660	285.8200
QC2EL	6.2004	1.00000	0.13226	-52.62200	697.3800	15.1270	221.0800
QC2EL2	7.2004	1.00000	0.13226	42.13200	706.6300	-13.6230	219.4600
DRIFT	8.2004	7.54870	7.54870	23.15900	213.7800	-20.0420	473.5800
QC3EL	15.7490	0.30000	-0.03516	15.64900	201.5800	-3.5201	479.3000
QC3EL2	16.0490	0.30000	-0.03516	8.81400	193.6200	13.0500	474.8700
DRIFT	16.3490	0.80000	0.80000	8.48890	179.7800	12.7620	454.2200
BH2EL	17.1490	0.40000	-0.00025	8.32640	173.0500	12.6180	444.0700
DRIFT	17.5490	26.00900	26.00900	-2.24350	14.8450	3.2345	31.7710
QC4EL	43.5580	0.30000	0.06077	-1.39090	15.9870	1.3256	30.5000
QC4EL2	43.8580	0.30000	0.06077	-0.43236	16.5790	-0.4981	30.3290
DRIFT	44.1580	5.36410	5.36410	-0.81638	23.2780	-0.7189	36.8570
BH5EL	49.5220	0.40000	-7.62E-5	-0.84502	23.9420	-0.7353	37.4390
DRIFT	49.9220	0.30000	0.30000	-0.86650	24.4560	-0.7477	37.8840
QC5EL	50.2220	0.30000	-0.04461	-1.99470	25.3390	0.9120	37.8780
QC5EL2	50.5220	0.30000	-0.04461	-3.23050	26.9290	2.5281	36.8840

Table 3: Parameters of the HER Version 102 95/06/28

Where	from IP(m)	Between	X/Y Slit	Aper(cm) (normal)	Aper(cm) (fill)
LER	3.9	BX4I,QC5I	X	1.0	2.6
LER	10.097	QC3I,QC2I	X	1.5	4.0
LER	14.867	QC3I,QC2I	X,Y	2.7, 0.4	7.3, 0.7
HER	7.762	QC4EL,BH2EL	X	0.5	1.4
HER	35.572	QC3EL,QC2EL	X	2.0	5.4
HER	42.122	QC3EL,QC2EL	X,Y	3.6, 1.0	9.7, 2.0

Table 4: Slits/Masks in LER and HER

Name	σ_x (acc)	σ_x (Turtle)	σ_y (acc)	σ_y (Turtle)
IP	0.008	0.008	0.0002	0.0010
QCSR	0.041	0.040	0.0365	0.0367
DRIFT	0.057	0.056	0.0393	0.0392
QC2I	0.252	0.247	0.0136	0.0136
QC2I2	0.271	0.264	0.0102	0.0102
DRIFT	0.271	0.262	0.0076	0.0076
QC3I	0.148	0.146	0.0190	0.0192
DRIFT	0.144	0.140	0.0203	0.0202
QC4I	0.152	0.150	0.0231	0.0232
DRIFT	0.148	0.145	0.0245	0.0246
QC5I	0.104	0.102	0.0350	0.0350
DRIFT	0.099	0.097	0.0358	0.0359
BX5I	0.098	0.096	0.0352	0.0352
DRIFT	0.097	0.096	0.0347	0.0347
BX4I	0.096	0.095	0.0341	0.0339
DRIFT	0.091	0.090	0.0300	0.0301

Table 5: Beam profiles predicted and simulated; LER Version 230 95/06/28

Name	σ_x (acc)	σ_x (Turtle)	σ_y (acc)	σ_y (Turtle)
IP	0.0080	0.0082	0.0002	0.0009
QCSLA	0.0326	0.0348	0.0288	0.0279
QCSLB	0.0399	0.0415	0.0337	0.0325
DRIFT	0.0908	0.0895	0.0464	0.0444
QC1EL	0.1043	0.1021	0.0480	0.0462
QC1EL2	0.1227	0.1183	0.0473	0.0454
DRIFT	0.3056	0.2903	0.0321	0.0309
QC2EL	0.3540	0.3376	0.0282	0.0274
QC2EL2	0.3566	0.3386	0.0281	0.0272
DRIFT	0.1962	0.1870	0.0413	0.0403
QC3EL	0.1905	0.1817	0.0415	0.0404
QC3EL2	0.1867	0.1778	0.0413	0.0404
DRIFT	0.1799	0.1703	0.0404	0.0394
BH2EL	0.1765	0.1764	0.0400	0.0391
DRIFT	0.0517	0.0511	0.0107	0.0105
QC4EL	0.0536	0.0530	0.0104	0.0103
QC4EL2	0.0546	0.0539	0.0102	0.0104
DRIFT	0.0647	0.0629	0.0115	0.0113
BH5EL	0.0656	0.0638	0.0116	0.0115
DRIFT	0.0663	0.0645	0.0117	0.0115
QC5EL	0.0675	0.0655	0.0117	0.0116
QC5EL2	0.0696	0.0677	0.0115	0.0116

Table 6: Beam profiles predicted and simulated : HER Version 102 95/06/28

Process	Cut(normal run)	Cut(injection)
	ϵ_c	ϵ_c
e^+ Brem	0.05	0.001
e^- Brem	0.05	0.001
	θ_c (Rad)	θ_c (Rad)
e^+ Coul	0.0005	0.0001
e^- Coul	0.0005	0.0001

Table 7: Values of physical cuts used in the generator

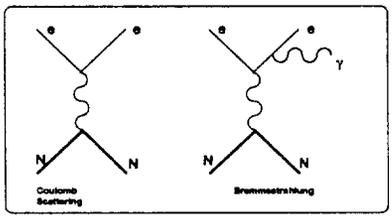

Figure 1: Feynman diagrams for Coulomb scattering and Bremsstrahlung of a beam electron(positron) off a residual gas nucleus.

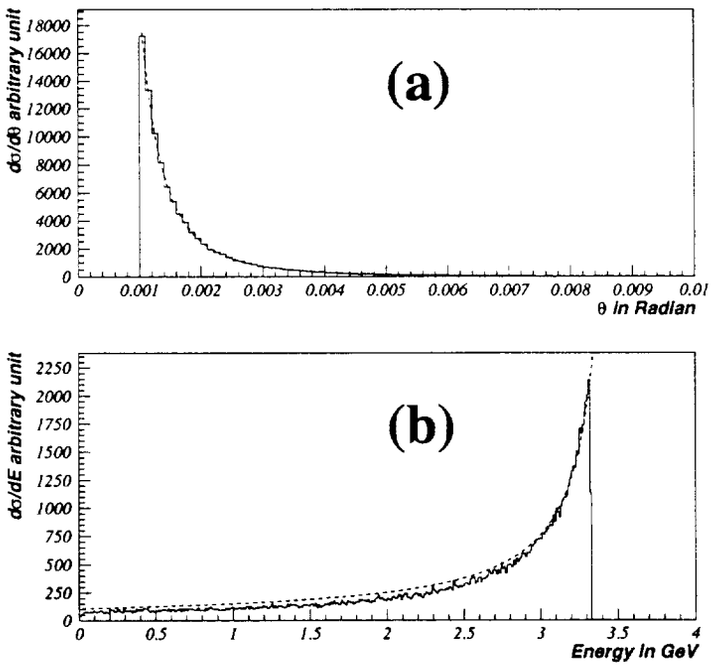

Figure 2: Differential cross-sections of spent positrons for (a) Coulomb scattering process and (b) Bremsstrahlung process. See text for details.

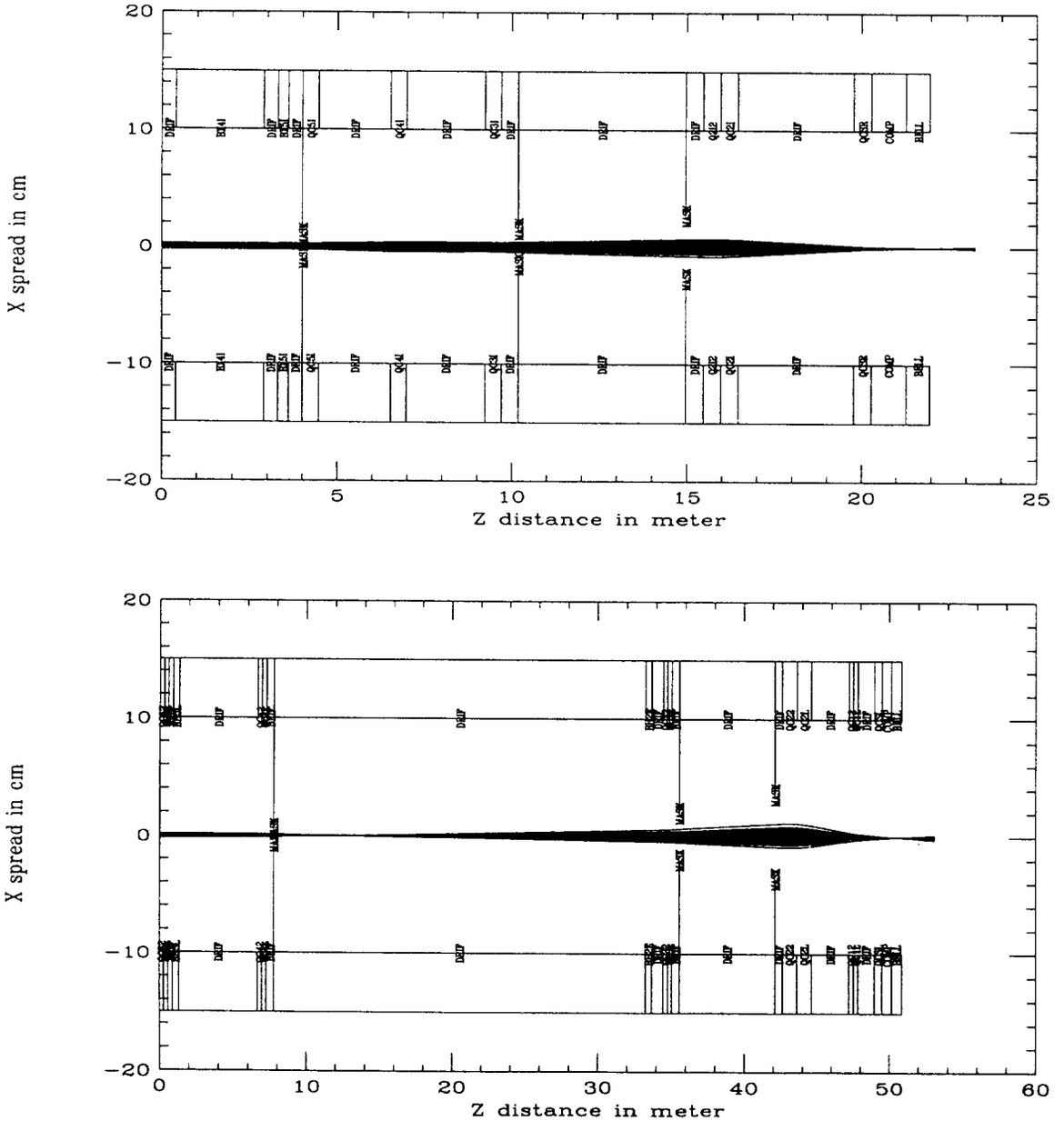

Figure 3: Beam propagation for no beam-gas scattering. Top : positron beam, Bottom : electron beam.

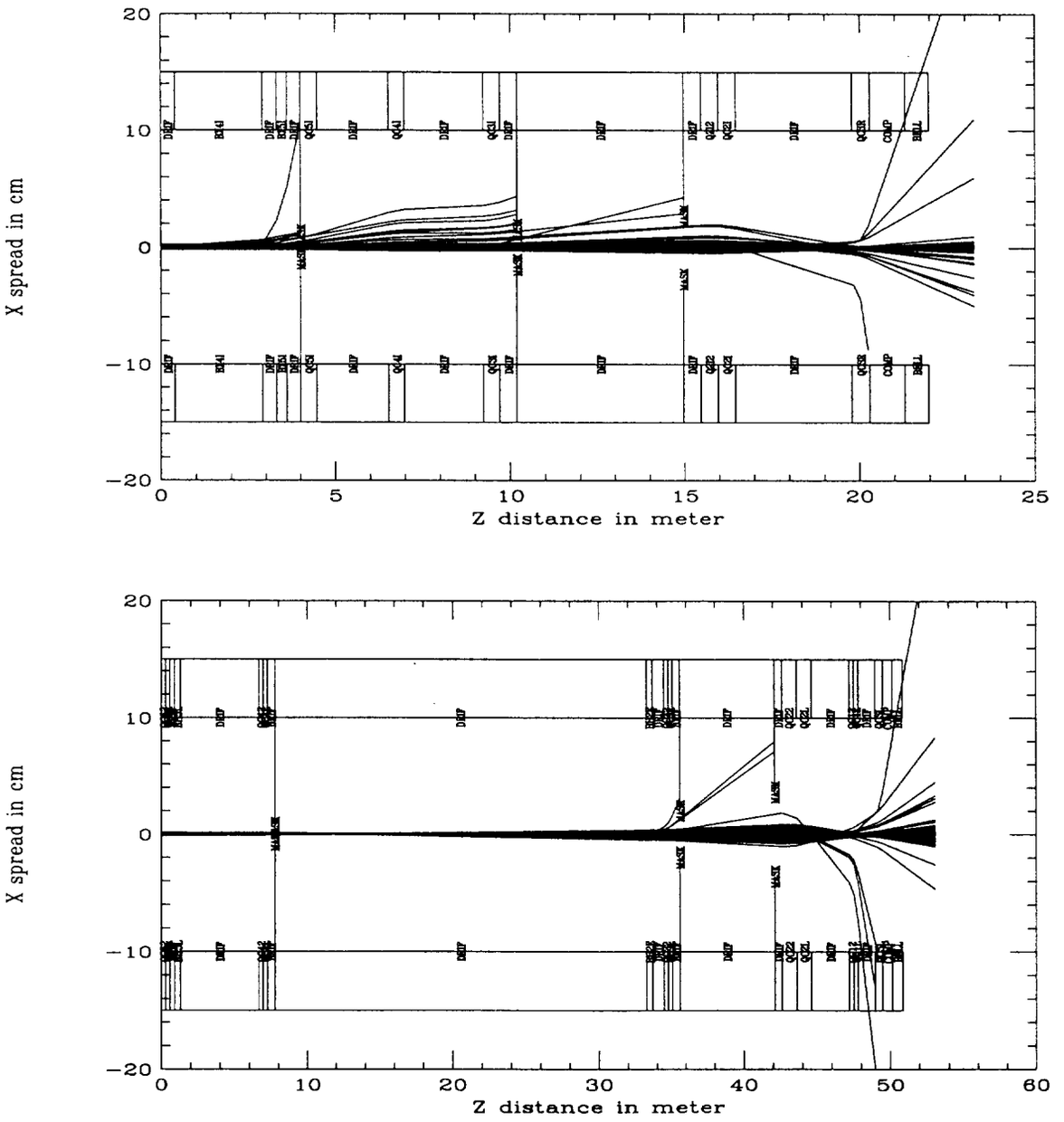

Figure 4: Beam propagation for beam particles that have undergone Bremsstrahlung process. Top : positron beam, Bottom : electron beam.

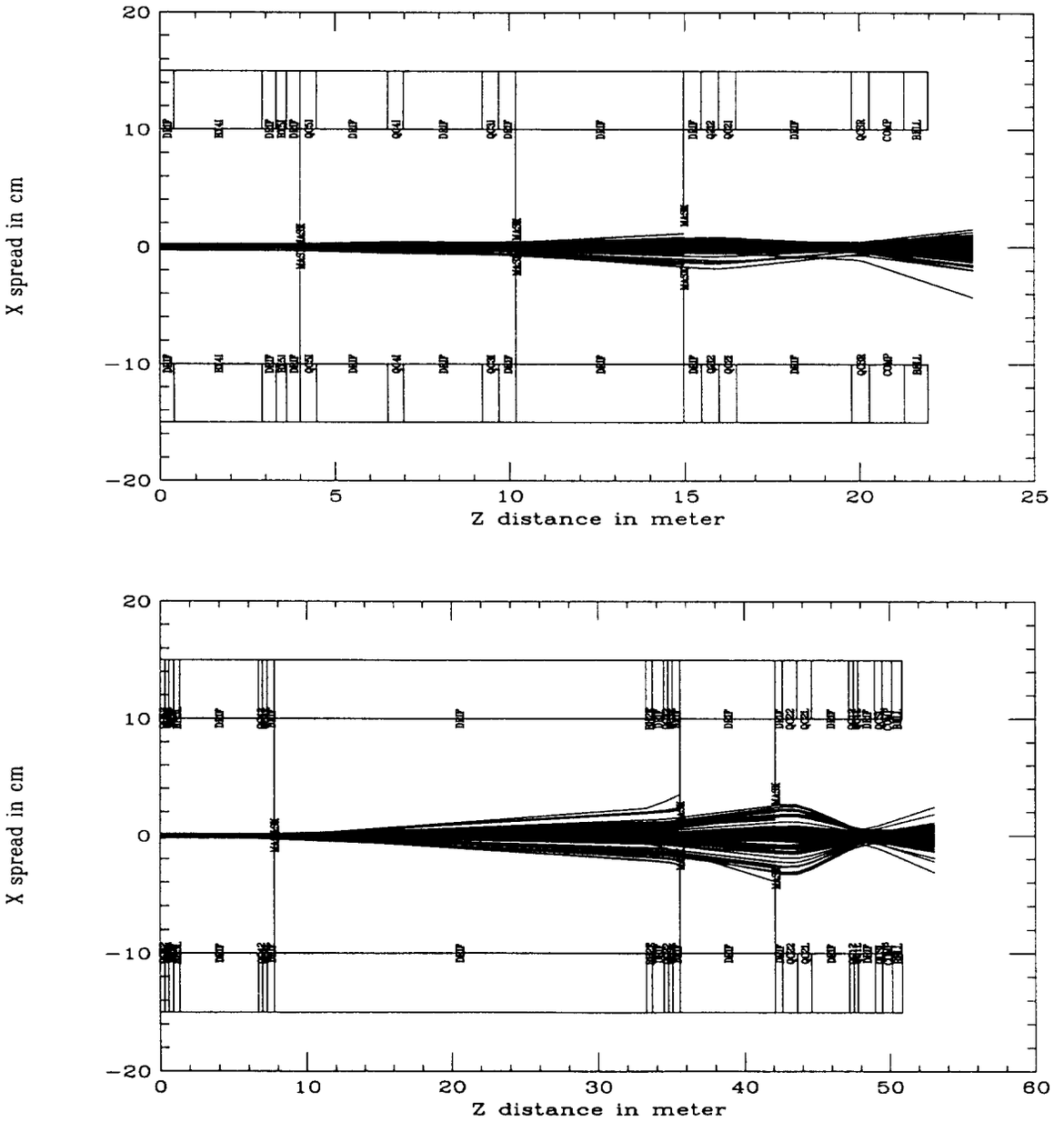

Figure 5: Beam propagation for beam particles that have undergone Coulomb scattering process. Top : positron beam, Bottom : electron beam.

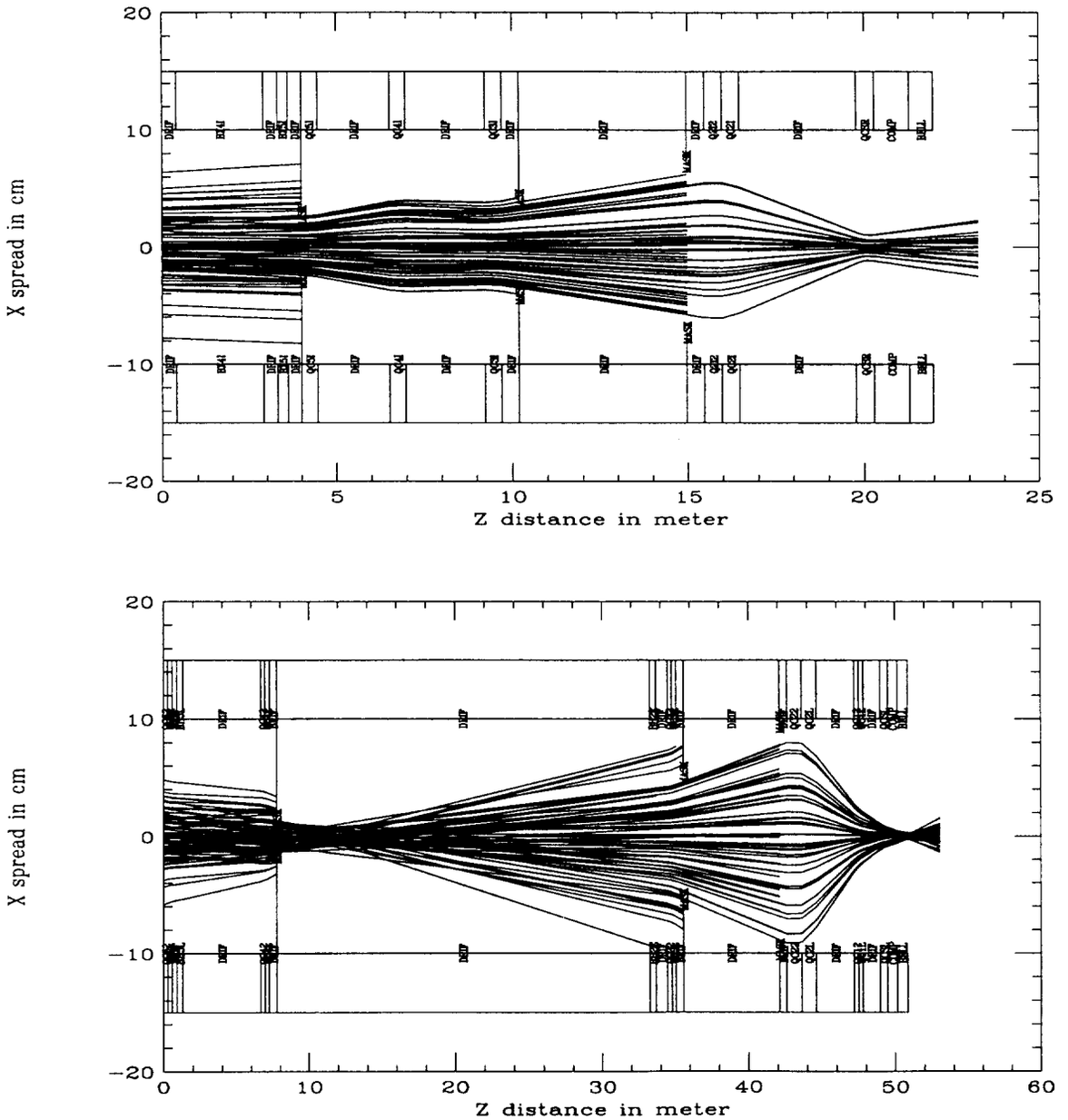

Figure 6: Injection time beam propagation for no beam-gas scattering. Top : positron beam, Bottom : electron beam.

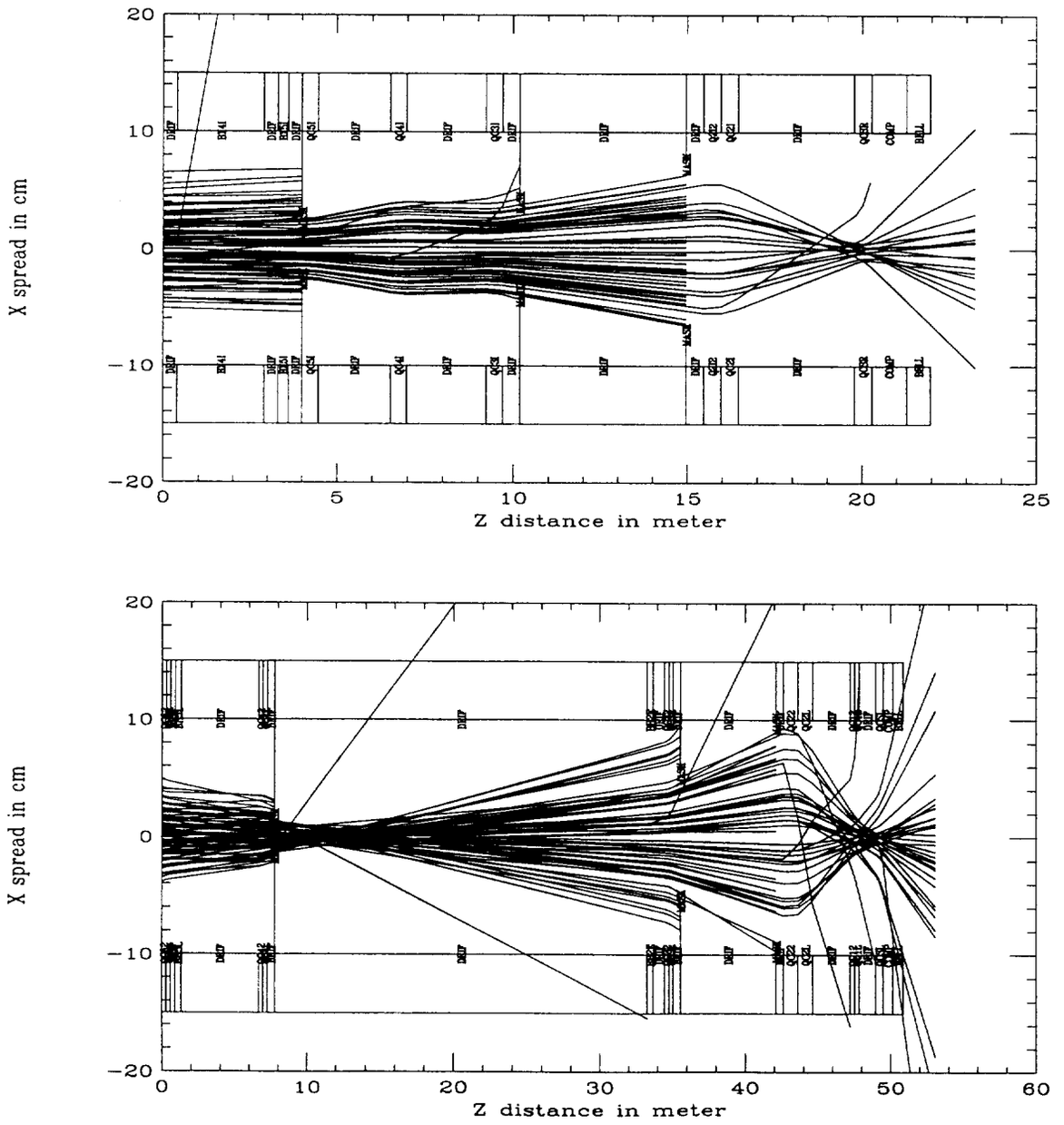

Figure 7: Injection time beam propagation for beam particles that have undergone Bremsstrahlung process. Top : positron beam, Bottom : electron beam.

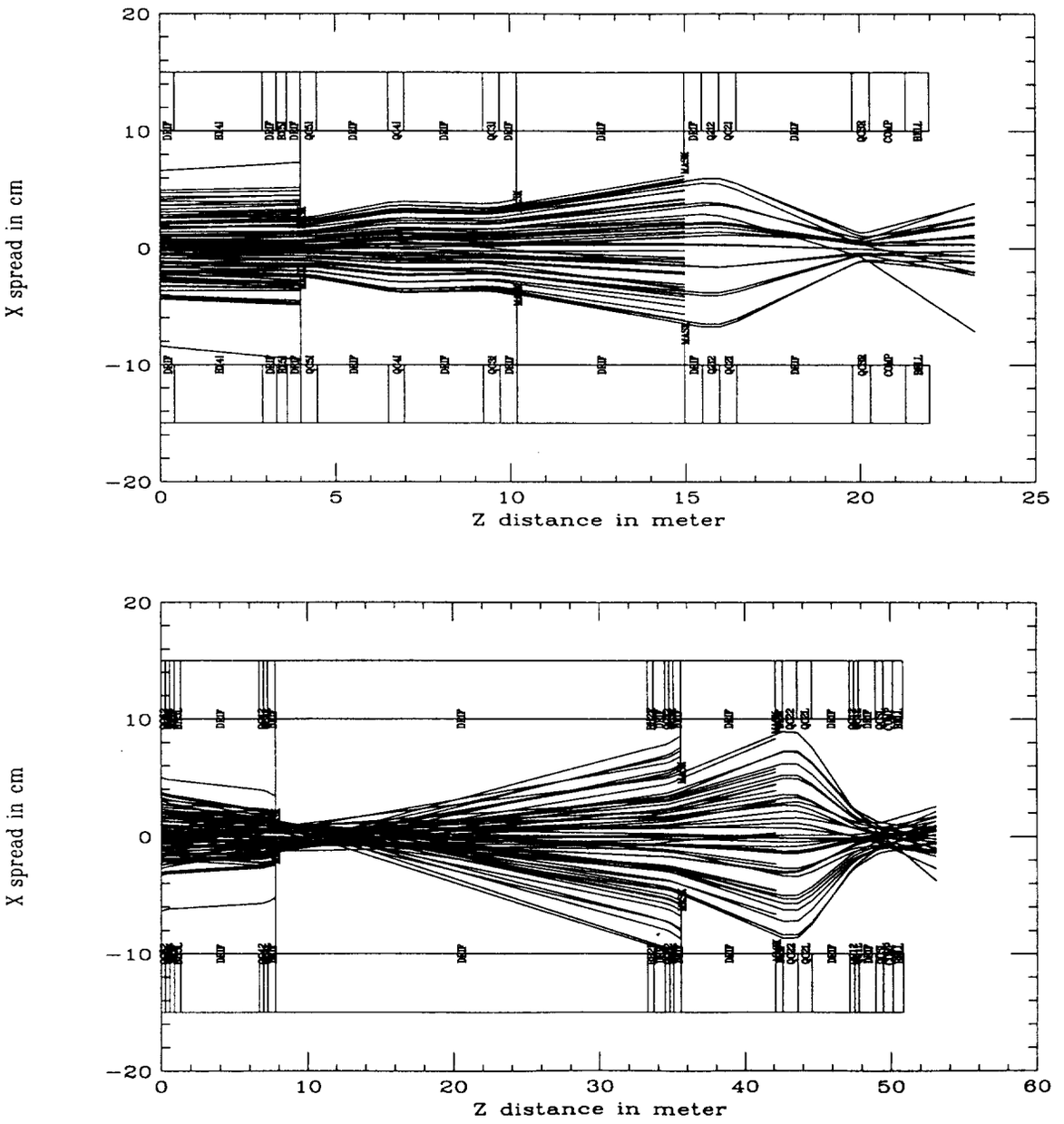

Figure 8: Injection time beam propagation for beam particles that have undergone Coulomb scattering process. Top : positron beam, Bottom : electron beam.

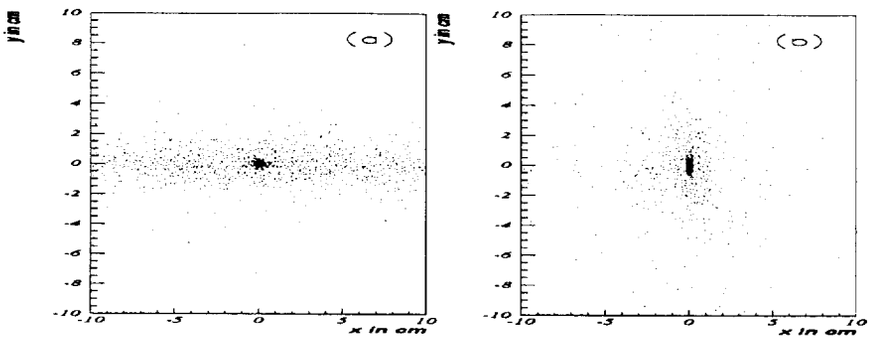

Figure 9: (a) Spent positron (e^+ Bremsstrahlung) profile at the interaction point; (b) same profile when the initial beam sampling is rotated by 90°. It is evident that the spent beam profile roughly follows the beam shape.

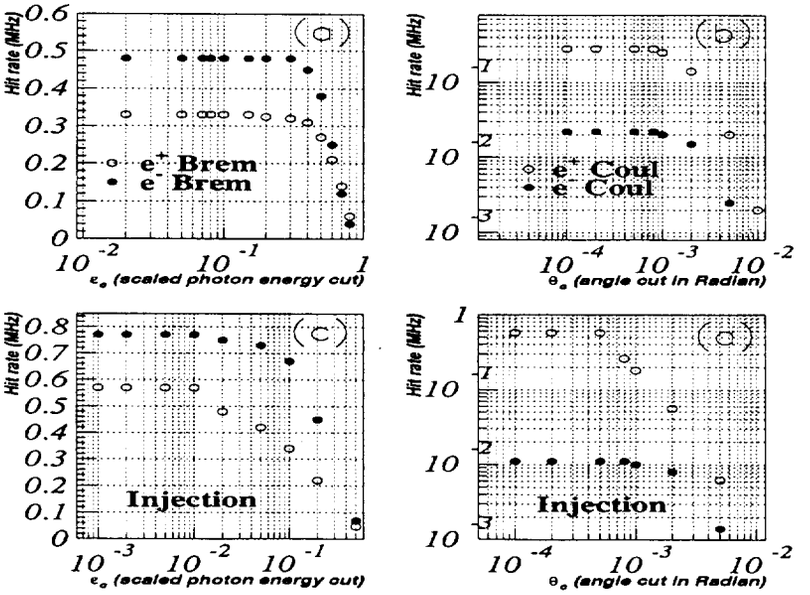

Figure 10: (a) and (c) : Hit rate as a function of scaled photon energy cut ϵ_c, for normal run-time and injection time, respectively; (b) and (d) : Hit rate as a function of minimum scattering angle cut θ_c, for normal run-time and injection time, respectively.

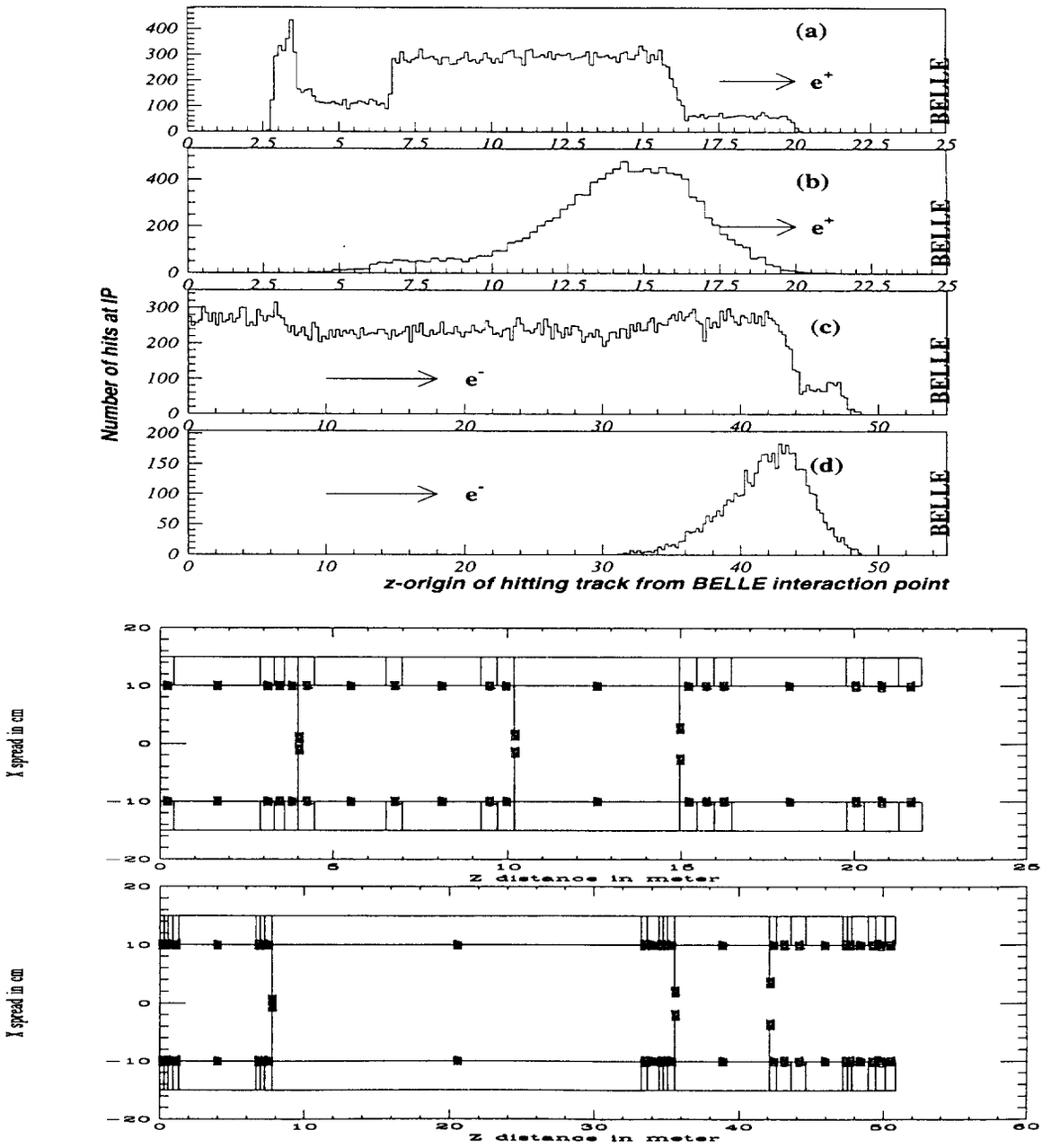

Figure 11: Distribution of z-origin of hitting spent beam particles along the beam-line. (a) e^+ Bremsstrahlung, (b) e^+ Coulomb, (c) e^- Bremsstrahlung and (d) e^- Coulomb scattering processes. Pictures of beam elements of LER and HER are given at the bottom as maps.

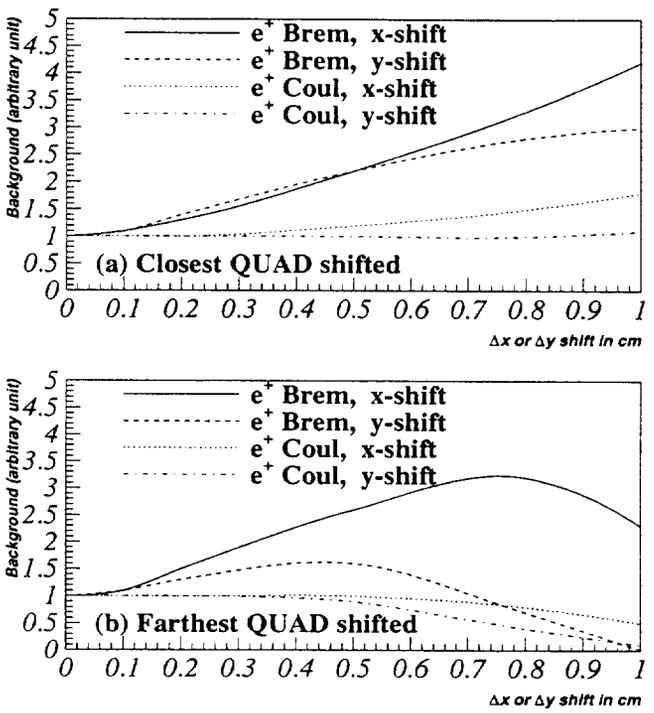

Figure 12: Increase by factor in background hit rate as a function of x- or y-shift in quadrupoles for LER; (a) when nearest quad from BELLE is shifted, (b) when farthest quad is shifted.

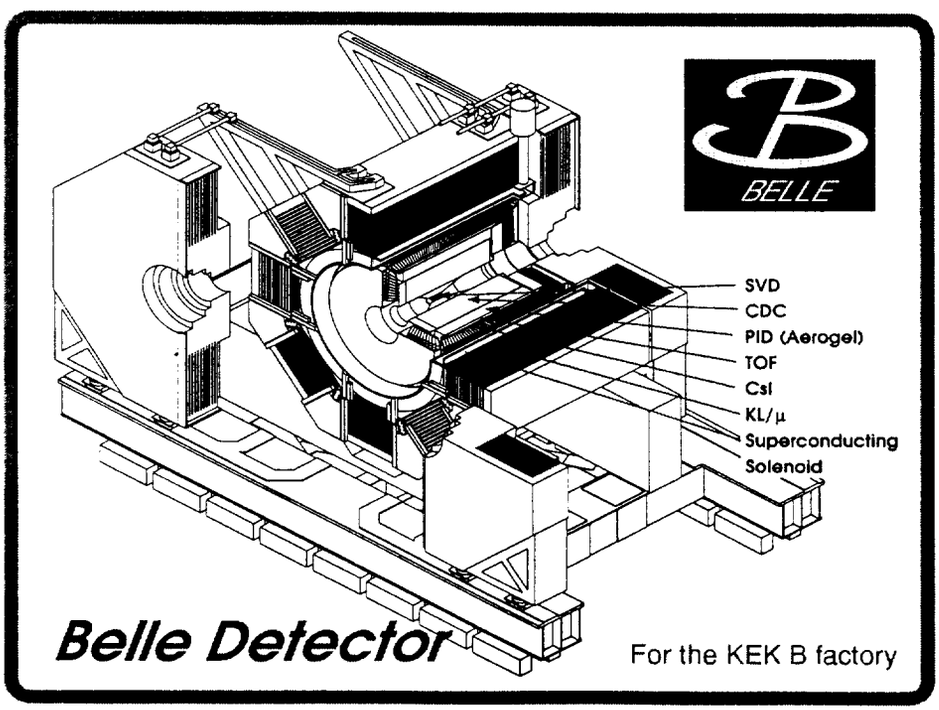

Figure 13: Schematic diagram of the BELLE detector.

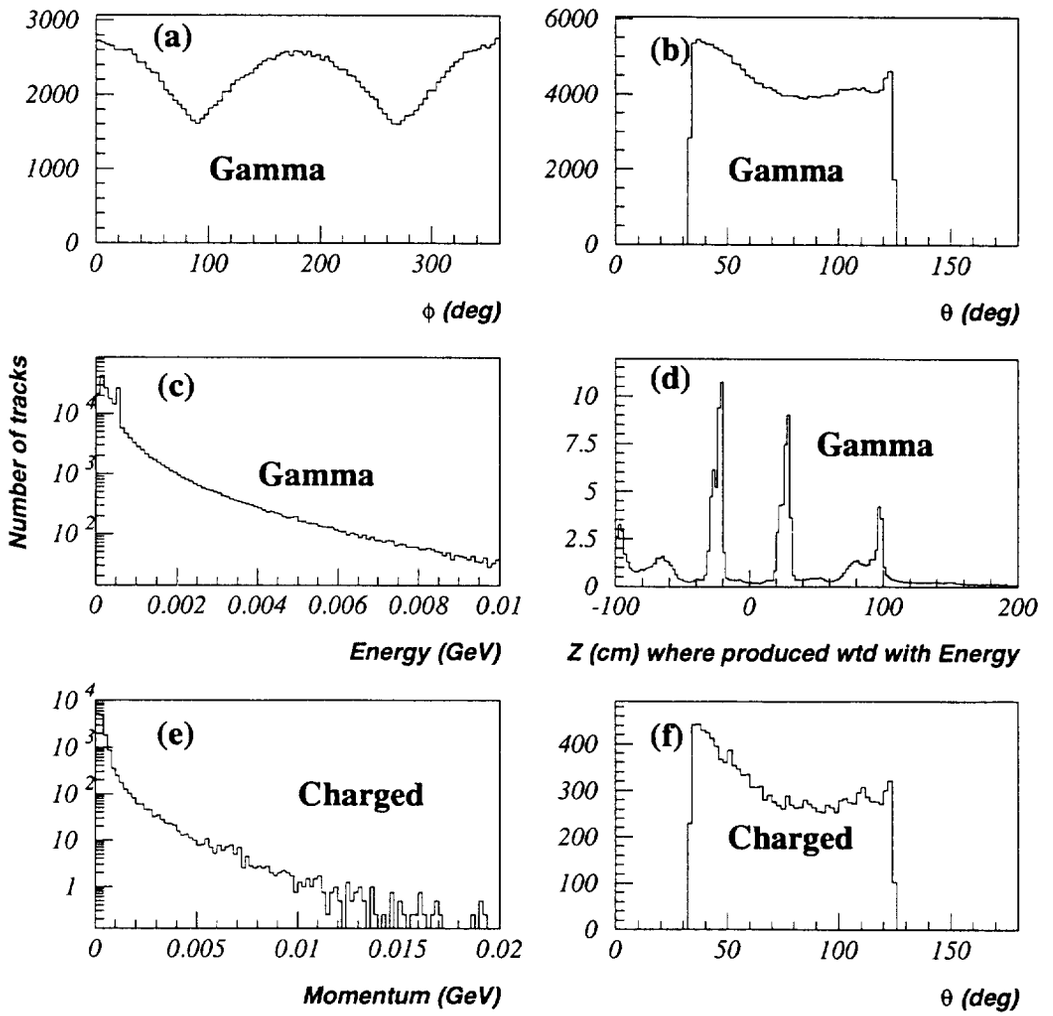

Figure 14: Profiles of background tracks entering the BELLE TOF. Number of tracks are accumulated in 10 milliseconds of normal machine operation. (a) azimuth of photons, (b) polar angle of photons, (c) Energy of photons, (d) z-distribution of the photons at their closest approach to beam-line, weighted with their energy (e) Momentum of charged particles and (f) polar angle of charged particles.